Voltammetric characterisation of the aerobic energy dissipating nitrate reductase of Paracoccus pantotrophus: exploring the activity of a redox balancing enzyme as a function of electrochemical potential

Andrew J Gates, David J Richardson, Julea N Butt

Voltammetric Characterisation of the Aerobic Energy Dissipating Nitrate Reductase of *Paracoccus pantotrophus*: Exploring the Activity of a Redox Balancing Enzyme as a Function of Electrochemical Potential.

Andrew J. Gates, David J. Richardson and Julea N. Butt[1]

Centre for Metalloprotein Spectroscopy and Biology,
School of Chemical Sciences and Pharmacy, School of Biological Sciences,
University of East Anglia, Norwich Research Park, Norwich, NR4 7TJ, UK

[1] Correspondence should be addressed to:
Dr Julea Butt
School of Chemical Sciences and Pharmacy
University of East Anglia, Norwich, NR4 7TJ, UK
Phone: +44 (0)1603 593877 Fax: +44 (0)1603 592003 E: j.butt@uea.ac.uk

Running title: *P. pantotrophus* periplasmic nitrate reductase

Synopsis.

Paracoccus pantotrophus expresses two nitrate reductases associated with respiratory electron transport, NapABC and NarGHI. Both enzymes derive electrons from ubiquinol to reduce nitrate to nitrite. However, while NarGHI harnesses the energy of the quinol/nitrate couple to generate a transmembrane proton gradient, NapABC dissipates the energy associated with these reducing equivalents. Here we explore the nitrate reductase activity of purified NapAB as a function of electrochemical potential, substrate concentration and pH using protein film voltammetry. Nitrate reduction by NapAB is shown to occur at potentials below ca. 0.1 V at pH 7. These are lower potentials than required for NarGH nitrate reduction. The potentials required for Nap nitrate reduction are also likely to require ubiquinol/ubiquinone ratios higher than are needed to activate the H^+-pumping oxidases expressed during aerobic growth where Nap levels are maximal. Thus, the operational potentials of *P. pantotrophus* NapAB are consistent with a productive role in redox balancing. A

Michaelis constant (K_M) of ca. 45 μM was determined for NapAB nitrate reduction at pH 7. This is in line with studies on intact cells where nitrate reduction by Nap was described by a Monod constant (K_S) of less than 15 μM. The voltammetric studies also disclosed maximal NapAB activity in a narrow window of potential. This behaviour is resistant to change of pH, nitrate concentration and inhibitor concentration and its possible mechanistic origins are discussed.

Keywords:

molybdenum, iron-sulphur cluster, heme, voltammetry, quinol-pool, nitrate reduction

Abbreviations:

$E^{o'}$, reduction potential at pH 7;

EPR, electron paramagnetic resonance;

i, catalytic current magnitude;

K_M, Michaelis constant;

K_S, Monod constant;

MGD, molybdopterin guanine dinucleotide;

Nap, periplasmic nitrate reductase;

Nar, membrane-bound nitrate reductase;

PFV, protein film voltammetry;

$UQ(H_2)$, ubiquinone (ubiquinol).

INTRODUCTION.

Paracoccus pantotrophus[1] has emerged as the paradigm organism for studies of aerobic nitrate respiration, a process now thought to be widespread amongst bacteria in which nitrate is used as an electron sink to facilitate redox balancing during oxidative metabolism of reduced carbon substrates [1,2]. In fact *P. pantotrophus* expresses two nitrate reductases associated with respiratory electron transport, Nap and Nar. These enzymes catalyse the same reaction,

$$NO_3^- + 2e^- + 2H^+ \rightarrow NO_2^- + H_2O$$

but they are distinguished by their cellular location, biochemistry and pattern of expression, Figure 1. Nar is expressed during anaerobic growth in the presence of nitrate. NarI, the membrane spanning di-heme subunit, acquires the electrons required for nitrate reduction from ubiquinol oxidation. Protons are released to the periplasm and electrons pass along a chain of iron-sulphur clusters in NarH and NarG to the site of nitrate reduction that is a Mo-*bis*-molybdopterin guanine dinucleotide cofactor (Mo[MGD]$_2$) with aspartate coordination [3,4]. The disposition of catalytic centres allows Nar to couple cytoplasmic nitrate reduction with 'periplasmic' quinol oxidation. As a consequence free energy associated with the ubiquinol/nitrate redox couple is conserved as a transmembrane proton electrochemical gradient [5].

In contrast to the expression of *nar*, Nap levels in *P. pantotrophus* are maximal during aerobic growth with the highly reduced carbon source butyrate [6]. Ubiquinol oxidation by Nap releases protons to the periplasm where nitrate reduction also occurs, Figure 1. Energy conservation is precluded and Nap is proposed to dissipate excess reducing equivalents from the ubiquinol pool. Thus, Nap is a redox balancing system that operates to poise the aerobic respiratory electron transport system to maximise growth rate. Nap, like Nar, employs three subunits to couple ubiquinol oxidation with nitrate reduction [1,2]. The membrane anchored tetra-heme cytochrome, NapC, catalyses ubiquinol oxidation. Hemes in NapB and an iron-sulphur cluster in NapA relay electrons to a cysteine coordinated Mo[MGD]$_2$ where nitrate reduction occurs [7].

Stable heterodimeric nitrate reductases, NarGH and NapAB, are formed from Nar and Nap respectively in the absence of their quinol oxidising subunits [8,9]. These soluble enzymes facilitate mechanistic studies of nitrate reduction and we have

[1] The α-proteobacterium formerly known as *Thiosphaera pantotropha* and *Paracoccus denitrificans* GB17.

shown that graphite electrodes can substitute for NarI to act as effective electron donors to *P. pantotrophus* NarGH [10-12]. Nitrate reduction driven by electrodic reduction of NarGH using protein film voltammetry (PFV) is characterised by a Michaelis constant (K_M) of ca. 20 μM. This compares favourably to the K_M of ca. 13 μM observed when quinol provides electrons to NarGHI and supports a functional analogy between the graphite electrode and the quinol oxidising subunit for studies of nitrate reduction [8,10]. The voltammetric studies offered additional information since they resolved NarGH activity across the electrochemical potential domain. At pH 7 NarGH was shown to be active below ca. 0.2 V and at potentials that should be readily accessible to the quinol pool during anaerobic respiration ($E^{o'}$ UQ/UQH_2 ca. 0.04 V) [13]. Two catalytically competent but kinetically distinct forms of NarGH were also disclosed and proposed to interconvert reversibly through redox transformation of an iron-sulphur cluster or the $Mo^{5+/4+}$ couple.

P. pantotrophus NapAB has not been studied by PFV although it has been the subject of extensive spectroscopic and kinetic analyses that have raised three important questions [9,14-19]. Firstly, NapA is closely related to a family of cytoplasmic nitrate reductases that are involved in anabolic, rather than catabolic, nitrate metabolism and the current view is that NapA evolved from a primordial cytoplasmic assimilatory enzyme [20]. In the case of the cytoplasmic assimilatory nitrate reductases these enzymes operate in the relatively reducing environment of the cytoplasm using electron donors such as ferredoxin or NAD(P)H that have reduction potentials in the region of -0.3 to -0.4 V. Evolution into a periplasmic respiratory enzyme required that Nap engage with quinolic electron donors having significantly higher reduction potentials. PFV of one assimilatory nitrate reductase, *Synecochoccus elongatus* NarB, showed that it became active below ca. -0.2 V [21]. Since *P. pantotrophus* NapA shares 70% sequence similarity with *S. elongatus* NarB, and all of the residues predicted to be essential for catalysis are conserved between the two enzymes, the question arises as to whether NapAB has evolved to operate in a higher potential domain than NarB and one that is more akin to the distinct, but quinol-dependent, NarGH enzyme?

The second important question about NapAB relates to its apparent affinity for nitrate. In *Escherichia coli*, NapA activity is associated with anaerobic rather than aerobic metabolism [22]. Studies of NarG and NapA mutants have led to the

suggestion that NapA represents a high affinity nitrate scavenging system that provides a selective advantage in nitrate-limited environments [23]. Measurements of the Monod constant (K_S) yield a value less than 20 μM for nitrate in a bacterial culture expressing *napA* but mutated in *nar*. Since NapA is periplasmic it is likely that this K_S reflects the K_M of the enzyme. However, spectrophotometric studies of nitrate reduction by purified *P. pantotrophus* NapAB gave a K_M of ca. 1000 μM [14,16]. This seems a high K_M given that *E. coli* NapA and *P. pantotrophus* NapA share 80% sequence similarity that includes a high degree of conservation for the active site residues. Thus, a reinvestigation of the kinetic properties of purified *P. pantotrophus* NapAB is warranted.

Finally, it is of interest to address whether NapAB exists in catalytically active but kinetically distinct forms that can be reversibly interconverted by a redox 'switch'. Such behaviour is displayed by NarGH(I) from *P. pantotrophus* and *E. coli*, in addition to *S. elongatus* NarB and *Rhodobacter sphaeroides* NapAB [10,21,24,25]. PFV is uniquely placed to address this issue, and those raised above, by defining *P. pantotrophus* NapAB activity as a function of electrochemical potential, substrate concentration and pH. Here we present results from such a study together with an analysis of Nap activity in intact cells of *P. pantotrophus*.

EXPERIMENTAL

NapAB purification

Samples of the purified periplasmic nitrate reductase, NapAB, were isolated independently from three separate growths of *P. pantotrophus* strain M6 [9]. Protein purification was by modification of the published method in which the order of the size-exclusion and Ni(II)-IMAC chromatographic steps were reversed [9]. The resulting samples were analysed by reducing SDS-PAGE. Gels stained for heme-linked peroxidase activity showed a single band at ~16 kDa consistent with the presence of NapB. Coomassie stained gels showed a single dominant band at ~90 kDa consistent with the presence of NapA and from which the NapAB samples were judged to be > 95% pure by densitometry. Purified, air equilibrated samples had A_{408nm}/A_{280nm} between 0.88 and 0.91 and concentrations were determined spectrophotometrically using ε_{408nm} = 220 mM^{-1} cm^{-1}. Purified enzyme was

exchanged into 20 mM Hepes, 500 mM NaCl, pH 7.5 containing 20% glycerol and stored as aliquots frozen in liquid N_2.

Nitrate reduction by Nap in intact cells of *P. pantotrophus*

Cells of *P. pantotrophus* strain M6 were suspended in 10 mM phosphate, 30 mM sodium succinate, 10 mM ammonium sulphate, pH 7 at a concentration of 0.5 mg dry weight mL^{-1}. The suspension was incubated anaerobically under a nitrogen atmosphere in a 5 mL reaction vessel at 30 ˚C that was stirred continuously with a magnetic flea. Pulses of nitrate (70 or 35 μM) were introduced to the vessel through stainless steel ports by injection from a Hamilton syringe and the nitrate concentration monitored with a nitrate electrode.

Analytical reagents

All solutions were prepared using Analytical Reagent grade water (Fisher Scientific, UK) and reagents of Analar, or higher, purity. The majority of voltammetric and potentiometric studies were performed in buffer-electrolyte solutions containing 100 mM NaCl and 25 mM of either glacial acetic acid, Mes, Pipes, Taps or Ches. Solution pH was adjusted to the desired value using aliquots of concentrated NaOH or HCl solutions. Where phosphate buffers were used these were prepared by titration of monobasic and dibasic potassium phosphate solutions to achieve the desired pH. Solutions containing defined concentrations of neomycin-B sulphate, KNO_3, NaN_3 and KSCN were prepared by dilution of concentrated, aqueous stock solutions with buffer-electrolyte. The pH of the resultant solutions, before and after experimentation, was confirmed to be that desired.

Spectrophotometric assays of nitrate reduction

Solution assays of NapAB activity were performed anaerobically at room temperature in 3.4 mL of 25 mM Pipes, 100 mM NaCl, pH 7.0 containing 1 mM reduced methyl viologen and the desired concentration of nitrate. Dithionite (typically 5 μL of a freshly prepared 17 mg mL^{-1} solution) was added to give a stable absorbance of ca. 1 at 600 nm and assays were initiated by addition of anaerobic NapAB to give a final concentration of 5.4 nM. Rates were calculated using ε_{600nm} = 13.7 mM^{-1} cm^{-1} for reduced methyl viologen.

Protein film voltammetry

Voltammetry was performed inside a Faraday cage housed in a N_2-filled chamber (atmospheric O_2 < 2 ppm) as described previously [10]. The glass electrochemical cell contained three electrodes and the sample chamber was maintained at 20 ^oC. The reference electrode was calomel (saturated KCl) and the working electrodes were pyrolytic graphite edge with a geometric surface area of 0.071 cm^2. Immediately prior to each experiment the working electrode surface was lightly abraded with 'Wet and Dry Abrasive Paper' of fine grade (English Abrasives and Chemicals Ltd, UK) and polished with an aqueous 0.3 μm Al_2O_3 slurry. After sonication, the electrode was rinsed, dried with a tissue and a few microlitres of ice-cold solution containing 5 μM NapAB and 2 mM neomycin-B sulphate as coadsorbate were placed on the electrode. After ca. 30 seconds, excess solution was removed from the electrode which was then immersed in the desired buffer-electrolyte. Potentials are quoted with respect to the standard hydrogen electrode (SHE) following addition of +0.241 V to the measured values.

Quantitative analysis of NapAB voltammetry was restricted to the pH range 5 to 9 where reproducible behaviour was observed. Catalytic currents were determined after subtraction of a 'baseline' film response recorded in the absence of nitrate. When comparing the magnitude of responses from different films this was done after normalising the response of each film to that measured in 2 mM nitrate, 2 mM neomycin, 25 mM Mes, 100 mM NaCl, pH 6 at 20 ^oC with a scan rate of 20 mV s^{-1} and electrode rotation at 3000 rpm. For kinetic analysis the catalytic currents from a nitrate titration were corrected for a first order loss of signal magnitude over the time of the experiment and then values of K_M and i_{max} were determined by regression in MicroCal Origin. Lineweaver-Burk and Hanes analyses gave results in good agreement with those from direct fit to the Michaelis-Menten equation. E_{cat} and E_{switch} were defined as the potentials of the maximum and minimum respectively in a plot of the first derivative of the baseline subtracted catalytic current with respect to applied potential. There was no discernable difference between NapAB PFV recorded in phosphate and Goods buffers for any given pH and nitrate concentration.

Potentiometric titrations

Mediated potentiometric titrations were performed in 25 mM Mes, 100 mM NaCl, pH 6.0 using modifications of method of Dutton with sodium dithionite as reductant and potassium ferricyanide as oxidant [26]. Full details are provided in the Supplementary Information. Variation of signal intensity with equilibration potential was fit to the Nernst equation with MicroCal Origin.

RESULTS

Defining catalytic PFV from NapAB

To assess the nitrate reductase activity of purified NapAB two microlitres of an ice-cold sample containing 5 μM enzyme and 2 mM neomycin were placed on a pyrolytic graphite 'edge' electrode. After a few seconds excess solution was removed and the electrode placed in buffer-electrolyte. Cyclic voltammetry with rapid electrode rotation showed a featureless response but the introduction of nitrate produced persistent negative currents below approximately 0.1 V, Figure 2. These negative currents reflected electrocatalytic reduction. Since control experiments showed the catalytic currents were not observed in the absence of enzyme or nitrate they were attributed to NapAB catalysed nitrate reduction driven by direct electron transfer from the electrode to NapAB.

The most striking feature of the catalytic response displayed by NapAB is the maximum, or 'peak', of activity observed at approximately -0.15 V, Figure 2. The peak reflects increased NapAB activity on first lowering the electrode potential followed by a region where activity drops to a constant lower level despite an increased driving force for the reaction that is catalysed. The peak of activity was observed, regardless of scan direction, during at least 30 minutes of continuous voltammetry and for three independent preparations of NapAB. The peak also persisted during catalysis at pH 5 through to pH 9 and for nitrate concentrations between 5 and 2000 μM. At more alkaline pH the smaller catalytic currents suggested lower enzyme activity. Nevertheless for all conditions investigated the maximum 'peak' activity was approximately twice that displayed by NapAB at -0.4 V where the nitrate reduction rate becomes independent of further increase of driving force, see for example Figure 3(A).

Neomycin is often used as a co-adsorbate in PFV. Its influence on the catalytic voltammetry of NapAB was assessed in experiments performed without neomycin present. These produced catalytic waves with shapes, position and initial magnitude in good agreement with those recorded when neomycin was present. However, the magnitude of the response was significantly more persistent in the presence of neomycin ($t_{½}$ ~ 20 mins rather than 8 mins in the absence of neomycin) and since this facilitated data collection and analysis neomycin was included in all further experiments. The catalytic wave shape was also found to be independent of the presence of 140 mM nitrite and variation of the electrode rotation rate between 2000 and 3000 rpm. These results showed that the response was free from limitations due to product inhibition or the rates of substrate delivery/product removal from the electrode surface. Thus, the peak of activity displayed by NapAB reflects reversible switching of the enzyme between catalytically active but kinetically distinct forms on traversing the electrochemical potential domain.

Kinetic analysis of NapAB nitrate reduction

The catalytic response from a NapAB film measured at 5 mV s^{-1} was found to superimpose on that measured at 100 mV s^{-1} with no sign of a smearing towards lower potentials that would be seen if the catalytic currents were limited by a range of sluggish interfacial electron exchange rates [27]. Thus, the kinetic parameters describing NapAB catalysis were obtained from direct analysis of the catalytic current magnitudes (i_{cat}) recorded in response to sequential nitrate additions, Figure 2. For each nitrate concentration catalytic current magnitudes were measured at the peak potential ($i_{cat}^{peak\,E}$) and -0.4 V ($i_{cat}^{-0.4V}$) then adjusted for the first-order loss of signal magnitude noted during each experiment. The results were fit to the Michaelis-Menten equation and values of K_M and the maximum catalytic current magnitude (i_{max}) determined for each potential, Figure 4. Catalytic currents could not be converted to turnover numbers since the amount of enzyme giving rise to the voltammetric response is unknown. However, the response of i_{max} to change of pH (or other experimental variable) quantitates the response of k_{cat} to such perturbations.

The values of $i_{\max}^{-0.4V}$ and $i_{\max}^{peak\,E}$ showed that NapAB activity was maximal at more acidic pH and decreased in a sigmoidal manner towards higher pH, Figure 3 (B). This behaviour was confirmed, and its reversibility established, when NapAB coated

electrodes were transferred between solutions of distinct pH in experiments which also demonstrated that the catalytic voltammetry originated from enzyme adsorbed on the electrode surface. The pH dependence of $i_{\max}^{-0.4V}$ and $i_{\max}^{peak\ E}$ were well-described by the equation

$$i_{\max} = \frac{\left(i_{\max}^{acid} \times 10^{-\mathrm{pH}}\right) + \left(i_{\max}^{alk} \times 10^{-\mathrm{p}K_a}\right)}{10^{-\mathrm{p}K_a} + 10^{-\mathrm{pH}}}$$

that relates modulation of NapAB activity to a single protonation event with pK_a = 7.8 ± 0.3 where i_{max}^{acid} is the maximal catalytic current in the acid limit and $i_{\max}^{alk}$ that in the alkaline limit, Figure 3 (B).

Inspection of the Michaelis constants for nitrate reduction showed $K_M^{peak\ E}$ was smaller than $K_M^{-0.4V}$ and that both values increased at higher pH, Figure 3 (C). Perhaps more significantly the values of $K_M^{peak\ E}$ and $K_M^{-0.4V}$ were 23 and 45 (± 5) μM respectively at pH 7. These are values considerably below that of approximately 1000 μM previously reported using dithionite reduced methyl viologen as electron donor so spectrophotometric analysis of the activity of these NapAB samples was also undertaken [9,14,16]. The assays were initiated by addition of NapAB and a rate acceleration, i.e., the appearance of a steeper absorbance *vs* time trace, was noted during every experiment, see for example the inset to Figure 5. These rate accelerations are significant because they reflect increased activity of NapAB as the methyl viologen becomes oxidised and the solution potential rises. The results are consistent with the peak of NapAB activity arising from intrinsic properties of the enzyme rather than the interfacial nature of the voltammetric experiment. This is an interpretation supported by the observation of peaked catalytic waves in PFV at basal plane graphite electrodes (not shown).

Analysis of the initial velocities from the spectrophotometric assays yielded K_M = 112 ± 12 μM and a turnover number of 58 ± 1 s^{-1}, Figure 5. Similar analysis for the steepest gradient in each assay gave a K_M of 176 ± 23 μM and turnover number of 104 ± 3 s^{-1}. Thus, the specificity constant (k_{cat}/K_M) for NapAB nitrate reduction is on the order of 6 x 10^5 M^{-1} s^{-1}. The K_M values obtained with the spectrophotometric assay are slightly higher than measured by PFV for the same enzyme sample but the results are within acceptable variation given the physical and chemical distinctions between

the two assay formats. The reason for the discrepancy between the present and previous spectrophotometric analyses is unclear but most importantly the K_M values defined here through two independent methods bring the kinetic description of *P. pantotrophus* NapAB into line with those for related enzymes [14,21,25].

To attempt to correlate the K_M values determined for the purified enzyme with that of the enzyme when it is operating in the intact cell with physiological electron donors, Nap nitrate reduction was monitored in whole cell suspensions of *P. pantotrophus* strain M6. This strain is a Tn5 insertion mutant deficient in the membrane-bound nitrate reductase Nar so that Nap is the only functional respiratory nitrate reductase [28]. In wild type cells *nap* expression is confined to aerobic growth on highly reduced carbon substrates. However, *P. pantotrophus* M6 also carries a point mutation in the *nap* promoter that leads to deregulation of the *nap* operon so that it is expressed under both anaerobic and aerobic conditions [29]. Since Nap is the only functional respiratory nitrate reductase in *P. pantotrophus* M6 then nitrate reduction by Nap in intact cells can be monitored by measuring nitrate disappearance from anaerobic cell suspensions using a nitrate electrode. The response of the nitrate electrode to nitrate was approximately linear in the 0 to 70 μM range. This is illustrated in Figure 6 where two pulses of nitrate (70 and 35 μM) are added to an anaerobic *P. pantotrophus* strain M6 cell suspension. The electron source was succinate, the catabolism of which results in electron input into the Q-pool via succinate dehydrogenase and NADH dehydrogenase with electrons then leaving the Q-pool via NapC. The maximum rate of nitrate reduction was 60 nmol min^{-1} mg $cells^{-1}$ and this was sustained until the nitrate concentration approached 15 μM. At this point the nitrate reduction rate decelerated, Figure 6. This indicated that the K_S of the cells for nitrate was <15 μM and similar to that estimated for intact cells of *Rhodobacter capsulatus* (<3 μM) and *E. coli* (<10 μM) expressing *nap* [23,30]. Since nitrate does not need to be transported across the cytoplasmic membrane for reduction by Nap to occur it is likely that the K_S of the cells reflects the K_M of Nap itself and for *P. pantotrophus* NapAB the low micromolar value of K_S is certainly in line with the PFV results.

Inhibition of NapAB nitrate reduction

Thiocyanate and azide have been shown to inhibit NapAB so nitrate titrations at a number of inhibitor concentrations were analysed at -0.09 and -0.40 V to assess the behaviour of the high- and low-potential enzyme forms respectively, see for example Figure 7 [14,16]. Lineweaver-Burk plots showed thiocyanate acted as a competitive inhibitor at both potentials by increasing K_M without affecting i_{max}, Figure 7 (A) and Supplementary Figure 1. Previous work reported the dissociation constant (K_d) for the thiocyanate:NapAB interaction as 4 ± 0.6 mM [16]. The K_d values calculated from this study are in good agreement with this, 6 (± 3) and 3 (± 2) mM at -0.09 and -0.40 V respectively, and show a similar affinity of thiocyanate for the high- and low-potential forms of NapAB [16]. Thus, the ratio of inhibited to uninhibited enzyme is defined by the ratio of thiocyanate to nitrate regardless of electrode potential and the wave shapes parallel those seen during nitrate titrations in the absence of thiocyanate, e.g., compare Figures 2 and 7 (A). In contrast, azide induces a change of catalytic wave shape, Figure 7 (B). A peak of activity is retained but inhibition of the high-potential form is more marked than inhibition of the low-potential form. Lineweaver-Burk plots indicate mixed inhibition at -0.09 and -0.40 V since both K_M and i_{max} were sensitive to azide concentration, Figure 7 (B) and Supplementary Figure 2. The plots failed to define a single intercept that would indicate complete (linear) inhibition [31,32]. This is consistent with the approach of i_{max} to a finite but non-zero value at the higher azide concentrations used in this study, Supplementary Figure 2, and suggests the presence of a catalytically competent NapAB:azide complex.

Correlating the NapAB catalytic voltammetry with cofactor reduction potentials

The catalytic wave defines windows of potential over which the activity of NapAB is modulated, up or down, as the potential is varied. The steepest point on each flank of the peak quantitates the potential of that part of the wave, E_{cat} for the high-potential flank and E_{switch} for the low-potential flank, Figure 2. At 2 mM nitrate E_{switch} varied linearly with pH and by -15 mV per pH unit, Figure 3 (D). E_{cat} showed a more complex pH dependence and one that indicates protonation of an oxidised form of the enzyme. If it is assumed that E_{cat} reflects the properties of a single redox couple within NapAB its pH dependence can be described by the equation

$$E_{cat} = E_{acid} + \frac{RT}{nF}\ln\left(\frac{1}{1+10^{pH-pK_a}}\right)$$

where E_{acid} is E_{cat} in the acid limit, pK_a describes the properties of ionisable site and n is the number of electrons associated with the redox event. The overlapping contributions to the catalytic wave shape preclude unambiguous assignment of the electron stoichiometry associated with E_{cat} so n = 1 was assumed to gain an approximation of pK_a and a good fit to the data was found with pK_a = 7.2 ± 0.1 and E_{acid} = 0.3 ± 0.01 V. At 5 µM nitrate the values of E_{cat} and E_{switch} were higher by ca. 50 and 100 mV respectively than those at 2 mM nitrate. However, the pH dependence of both E_{cat} and E_{switch} at 5 µM nitrate was similar to their respective behaviours at 2 mM nitrate. These results suggest that the ionising residues responsible for the modulation of E_{cat} and E_{switch} are accessible in both the free enzyme and Michaelis complex and may not form integral parts of the nitrate reduction site.

A comparison of E_{cat}, E_{switch} and the reduction potentials of centres within NapAB can provide a basis for considering possible origins of its distinctive catalytic properties. Previous studies have determined heme reduction potentials at pH 7.4 and the $[4Fe\text{-}4S]^{2+/1+}$ reduction potential at pH 7.0, Table 1. To complement these values and assess the properties of NapAB used in this study we performed potentiometric titrations at pH 6 where NapAB is most active (Supplementary Figures 3 and 4). Heme reduction was monitored by UV-visible absorption spectroscopy and reduction of the $[4Fe\text{-}4S]^{2+}$ cluster was followed by electron paramagnetic resonance (EPR) spectroscopy. The results are summarised in Table 1 where it is seen that the hemes have higher reduction potentials than the [4Fe-4S] cluster and that each of these redox transitions occurs in the range of potentials where modulations of NapAB activity are detected. In an attempt to assess active site redox chemistry we also measured EPR spectra of our samples at 66 K where signals arising from Mo^{5+} species are visible [14,19]. As in previous studies, a number of signals were detected none of which had an intensity that accounted for more than ca. 30% of Mo in the sample despite full Mo loading [9].

DISCUSSION

Bacterial nitrate reductases divide into two structural groups, those for which the protein ligand to the molybdenum ion originates from an aspartate residue, the Nar

group, and those for which it arises from a cysteine residue, the Nap and Nas enzymes [4]. The Nap and Nar enzymes receive electrons from the quinol pool which for *P. pantotrophus* is comprised of ubiquinol and ubiquinone. Here we see that NapAB activity is turned on below approximately 0.15 V and so, like NarGH, its operational potentials appear well-matched to the properties of the ubiquinol electron donor, Figure 8. Interesting comparison can be made with the assimilatory nitrate reductase (NarB) from *S. elongatus*. NarB activity is switched on below approximately -0.2 V and at potentials well-matched to the NAD^+/ NADH couple ($E^{o'}$ ~ -0.32 V) via which electrons from sugar oxidation are passed to cytoplasmic reductive metabolisms [21]. Thus, the activities of these enzymes appear to be tuned to reflect their source of electrons rather than the immediate Mo coordination sphere. In this light it is interesting to note that NapA is thought to have evolved from the cytoplasmic eubacterial assimilatory enzymes [20]. In this evolutionary view the primordial 'cytoplasmic' enzyme became fused to a TAT signal peptide that allowed its translocation to the periplasm and extra proteins, NapB and NapC, were recruited to allow communication with quinol. If our observations to date are generally applicable this evolution was also accompanied by a positive shift of enzyme operating potential.

When the periplasmic respiratory system of *P. pantotrophus* is considered as a whole it is notable that the three denitrification enzymes with periplasmic, or periplasmic facing, active sites are coupled to electron transfer at a point downstream of the cytochrome bc_1-complex [1]. Thus, the cytochrome cd_1 nitrite reductase, the integral membrane nitric oxide reductase and the nitrous oxide reductase accept electrons from either reduced cytochrome c_{550} or pseudoazurin ($E^{o'}$ ~ 0.25 V) generated by the cytochrome bc_1 complex in protonmotive processes. Here we find that the operating potential of NapAB is sufficiently positive to allow it to couple into the respiratory chain at the level of the quinol pool but not sufficiently high to allow it to operate upstream of cytochrome c_{550} and pseudoazurin. Thus, NapAB activity cannot be coupled into the cytochrome bc_1-complex protonmotive activity.

Closer inspection of the activity-potential profiles for *P. pantotrophus* NapAB and NarGH in 4 μM nitrate and at pH 6 and 7 shows that lower potentials are required to activate NapAB nitrate reduction, Figure 8. Indeed, lower potentials are required to activate NapAB than NarGH in like-for-like comparisons and while it is difficult to know the environments in which each nitrate reductase will operate some further

observations can be made if these general properties are related to potentials that may be imposed by the UQ/UQH_2 pool, Figure 8. From a thermodynamic perspective any reduction of the Q-pool would appear to be sufficient to drive nitrate reduction by NarGH. This seems a sensible scenario given that Nar is deployed to catalyse the first step of denitrification and drive energy conservation during anaerobic respiration in the presence of nitrate. By contrast NapAB will only become active when higher quinol levels are generated, consistent with the role of NapAB in dissipating excess reducing equivalents from the cytoplasmic membrane during aerobic respiration [1,2].

Unregulated electron flux through Nap would be detrimental to the cell as it would result in an unnecessary waste of redox energy. Three energy conserving, H^+-translocating oxidases are present during aerobic respiration by *P. pantotrophus* when *nap* is expressed [33]. The cytochrome aa_3- and cytochrome cbb_3-type oxidases receive electrons from UQH_2 via soluble cytochromes and the cytochrome bc_1-complex with the consequence that six protons are moved across the cytoplasmic membrane for each UQH_2 oxidised. In contrast, the cytochrome bo_3-type oxidase reacts directly with UQH_2 to move four protons across the membrane for each UQH_2 oxidised. Oxygen reduction by the cytochrome bc_1-complex dependent oxidases was shown to occur when the UQH_2 content of *P. pantotrophus* membranes rose above ca. 15 % and it is likely that turnover of the cytochrome bc_1-complex and hence these oxidases will become limited by UQ availability at very high UQH_2/UQ ratios [33]. The cytochrome bo_3-type quinol oxidase became active when the UQH_2 content exceeded 25%. Thus, our detection of significant (> 25 %) NapAB nitrate reductase activity at potentials that correlate with a UQH_2 content of approximately 25 % is entirely consistent with the role of NapAB in productive redox balancing. In the presence of highly reducing carbon substrates the levels of NapAB and the cytochrome bo_3-type quinol oxidase are upregulated and this genetic regulation appears to be complemented by the biochemistry of the enzymes to provide opportunities for rapid, finely tuned response to change of metabolism/respiratory pathway.

The K_S and K_M reported here for *P. pantotrophus* NapAB nitrate reduction place the apparent affinity of this enzyme for its substrate in line with those of homologous enzymes [21,23,25]. The ability of NapAB to convert reversibly between two catalytically competent but kinetically distinct forms on traversing the electrochemical potential domain is also a property shared with other Mo[MGD]$_2$-

enzymes [10,21,24,25,34]. However, the conditions under which this behaviour is displayed and the mechanistic implications depend on the identity of the enzyme. In one mechanism the $Mo^{5+/4+}$ couple is proposed to act as a redox 'switch' converting the enzyme between kinetically distinct forms [10,24,25,34]. Here, the higher-activity enzyme form present at more positive potentials arises from substrate (proton or nitrate) binding to the Mo^{5+} state. Increasingly negative potentials and/or lower substrate concentrations favour Mo^{4+} formation prior to substrate binding and catalysis proceeds via a slower pathway that results in attenuated catalytic rates. Thus, higher substrate concentrations are predicted to favour substrate binding to Mo^{5+} and produce an increasingly sigmoidal catalytic wave shape that will ultimately reflect reduction of the $Mo^{5+/4+}$ couple in substrate bound enzyme. Such behaviour is seen in the pH dependence of the catalytic PFV from *E. coli* dimethyl sulfoxide reductase and the nitrate dependence of the catalytic responses from *S. elongatus* NarB and NarGH(I) of *E. coli* and *P. denitrificans*. By contrast the *P. pantotrophus* NapAB wave shape is remarkably resilient to change of pH and nitrate concentration.

It is difficult to relate the activities seen here to active site redox chemistry in the absence of reduction potentials for a significant population of the NapAB sample and as an aside it is worth noting that the failure to detect significant Mo^{5+} EPR intensities in potentiometric studies may indicate that much of the sample moves between Mo^{6+} and Mo^{4+} over a narrow potential window. However, preferential nitrate binding to *E. coli* NarGH in the Mo^{5+} state was also inferred from voltammetry in the presence of the competitive inhibitor azide [24]. Azide inhibited the high-potential enzyme form with a greater potency than displayed for the low-potential enzyme form and the catalytic wave shape changed from peaked to sigmoidal. This was taken to reflect the higher affinity of azide for Mo^{5+} than Mo^{4+} expected from electrostatic considerations and it was proposed that nitrate would behave similarly. Thiocyanate is a competitive inhibitor of *P. pantotrophus* NapAB and previous spectroscopic studies have provided evidence for thiocyanate (S) coordination to the Mo [16]. However, the NapAB catalytic wave shape was unaffected by the presence of thiocyanate providing no indication that thiocyanate discriminates between the catalytically active oxidation states. It could be argued that thiocyanate as a soft ligand is less discriminating than azide in its affinity for Mo oxidation states. However, that azide, a partial mixed inhibitor, of NapAB produces a clear change in

catalytic wave shape suggests that the peak of activity may not simply arise from preferential substrate binding to Mo^{5+} in this enzyme.

Alternate switching mechanisms can be proposed from more generic consequences of redox modulation within an enzyme. Here it is worth noting that peaked catalytic waves are not specific to Mo enzymes and they have been observed in multi-centred reductases with flavin- and heme-containing active sites [35-38]. For these enzymes attenuation of activity has been associated with conformational change driven by active site reduction and the consequences of reduction at redox centres remote from the active site. For NapAB such changes could be driven by redox chemistry at the active site or the [4Fe-4S] cluster whose reduction potential lies in the vicinity of E_{switch}. Substantial conformational change is unlikely to account for the modulated rate since this may be expected to occur at a slower rate than catalysis such that increasing the voltammetric scan rate would produce an increasingly sigmoidal wave as the attenuation is 'tuned-out'. This was not observed for NapAB where the entire catalytic response was compromised at scan rates above ca. 100 mV s^{-1}. Extended X-ray absorption fine structure of ferricyanide oxidised and dithionite reduced *P. pantotrophus* NapAB has suggested a lower S coordination of Mo^{4+} than Mo^{6+} that could result in modulation of the catalytic rate [14]. Alternatively the activity may be modulated by movement of an amino acid and/or a change of pK_a that affects proton and/or electron transfer events associated with catalysis. Such perturbations could impact catalysis via sites that are not immediately involved in nitrate coordination and it is interesting that the presence of azide, a partial inhibitor of NapAB, perturbs the wave shape for nitrate reduction.

In conclusion, we have presented results that demonstrate the high apparent affinity of *P. pantotrophus* NapAB towards its substrate nitrate. The mechanistic details that underpin the peak of activity displayed by this enzyme remain to be defined. However, it is apparent that the operational potentials of NapAB are well-placed to allow for effective redox balancing by dissipation of excess reducing equivalents during anaerobic growth of *P. pantotrophus*.

Acknowledgements

We are grateful to Ann Reilly for NapAB purification, Dr Myles Cheesman for assistance with EPR spectroscopy and to Gemma Kemp for fruitful discussions. AJG was funded by EPSRC through DTA and financial support for the project was

provided from the UK Biotechnology and Biological Sciences Research Council (grants 83/17233 and 83/13842) and a JIF award (062178).

References

[1] Richardson, D. J. (2000) Bacterial respiration: A flexible process for a changing environment. Microbiology **146**, 551-571

[2] Richardson, D. J., Berks, B. C., Russell, D. A., Spiro, S. and Taylor, C. J. (2001) Functional, biochemical and genetic diversity of prokaryotic nitrate reductases. Cell. Molec. Life Sci. **58**, 165-178

[3] Bertero, M. G., Rothery, R. A., Boroumand, N., Palak, M., Blasco, F., Ginet, N., Weiner, J. H. and Strynadka, N. C. J. (2005) Structural and biochemical characterization of a quinol binding site of *Escherichia coli* nitrate reductase A. J. Biol. Chem. **280**, 14836-14843

[4] Jormakka, M., Richardson, D., Byrne, B. and Iwata, S. (2004) Architecture of NarGH reveals a structural classification of Mo-*bis*MGD enzymes. Structure **12**, 95-104

[5] Parsonage, D. and Ferguson, S. J. (1983) Reassessment of pathways of electron flow to nitrate reductase that are coupled to energy-conservation in *Paracoccus denitrificans*. FEBS Lett. **153**, 108-112

[6] Sears, H. J., Spiro, S. and Richardson, D. J. (1997) Effect of carbon substrate and aeration on nitrate reduction and expression of the periplasmic and membrane-bound nitrate reductases in carbon-limited continuous cultures of *Paracoccus denitrificans* pd1222. Microbiology **143**, 3767-3774

[7] Arnoux, P., Sabaty, M., Alric, J., Frangioni, B., Guigliarelli, B., Adriano, J. M. and Pignol, D. (2003) Structural and redox plasticity in the heterodimeric periplasmic nitrate reductase. Nature Struct. Biol. **10**, 928-934

[8] Craske, A. and Ferguson, S. J. (1986) The respiratory nitrate reductase from *Paracoccus denitrificans* - molecular characterization and kinetic properties. Eur. J. Biochem. **158**, 429-436

[9] Berks, B. C., Richardson, D. J., Robinson, C., Reilly, A., Aplin, R. T. and Ferguson, S. J. (1994) Purification and characterization of the periplasmic

nitrate reductase from *Thiosphaera pantotropha*. Eur. J. Biochem. **220**, 117-124

[10] Anderson, L. J., Richardson, D. J. and Butt, J. N. (2001) Catalytic protein film voltammetry from a respiratory nitrate reductase provides evidence for complex electrochemical modulation of enzyme activity. Biochemistry **40**, 11294-11307

[11] Anderson, L. J., Richardson, D. J. and Butt, J. N. (2000) Using direct electrochemistry to probe rate limiting events during nitrate reductase turnover. Faraday Discuss. 155-169

[12] Field, S. J., Thornton, N. P., Anderson, L. J., Gates, A. J., Reilly, A., Jepson, B. J. N., Richardson, D. J., George, S. J., Cheesman, M. R. and Butt, J. N. (2005) Reductive activation of nitrate reductases. Dalton Trans. 3580-3586

[13] Nicholls, D. G. (1982) Bioenergetics: An introduction to the chemiosmotic theory. London: Academic Press Ltd

[14] Butler, C. S., Charnock, J. M., Bennett, B., Sears, H. J., Reilly, A. J., Ferguson, S. J., Garner, C. D., Lowe, D. J., Thomson, A. J., Berks, B. C. and Richardson, D. J. (1999) Models for molybdenum coordination during the catalytic cycle of periplasmic nitrate reductase from *Paracoccus denitrificans* derived from EPR and EXAFS spectroscopy. Biochemistry **38**, 9000-9012

[15] Breton, J., Berks, B. C., Reilly, A., Thomson, A. J., Ferguson, S. J. and Richardson, D. J. (1994) Characterization of the paramagnetic iron-containing redox centers of *Thiosphaera pantotropha* periplasmic nitrate reductase. FEBS Lett. **345**, 76-80

[16] Butler, C. S., Charnock, J. M., Garner, C. D., Thomson, A. J., Ferguson, S. J., Berks, B. C. and Richardson, D. J. (2000) Thiocyanate binding to the molybdenum centre of the periplasmic nitrate reductase from *Paracoccus pantotrophus*. Biochem. J. **352**, 859-864

[17] Butler, C. S., Ferguson, S. J., Berks, B. C., Thomson, A. J., Cheesman, M. R. and Richardson, D. J. (2001) Assignment of haem ligands and detection of electronic absorption bands of molybdenum in the di-haem periplasmic nitrate reductase of *Paracoccus pantotrophus*. FEBS Lett. **500**, 71-74

[18] Butler, C. S., Fairhurst, S. A., Ferguson, S. J., Thomson, A. J., Berks, B. C., Richardson, D. J. and Lowe, D. J. (2002) Mo(V) co-ordination in the periplasmic nitrate reductase from *Paracoccus pantotrophus* probed by

electron nuclear double resonance (ENDOR) spectroscopy. Biochem. J. **363**, 817-823

[19] Bennett, B., Berks, B. C., Ferguson, S. J., Thomson, A. J. and Richardson, D. J. (1994) Mo(V) electron paramagnetic resonance signals from the periplasmic nitrate reductase of *Thiosphaera pantotropha*. Eur. J. Biochem. **226**, 789-798

[20] Jepson, B. J. N., Marietou, A., Mohan, S., Cole, J. A., Butler, C. S. and Richardson, D. J. (2006) Evolution of the soluble nitrate reductase: Defining the monomeric periplasmic nitrate reductase subgroup. Biochem. Soc. Trans. **34**, 122-126

[21] Jepson, B. J. N., Anderson, L. J., Rubio, L. M., Taylor, C. J., Butler, C. S., Flores, E., Herrero, A., Butt, J. N. and Richardson, D. J. (2004) Tuning a nitrate reductase for function - the first spectropotentiometric characterization of a bacterial assimilatory nitrate reductase reveals novel redox properties. J. Biol. Chem. **279**, 32212-32218

[22] Potter, L., Angove, H., Richardson, D. and Cole, J. (2001) Nitrate reduction in the periplasm of gram-negative bacteria. Adv. Microb. Phys. 45, 51-112

[23] Potter, L. C., Millington, P., Griffiths, L., Thomas, G. H. and Cole, J. A. (1999) Competition between *Escherichia coli* strains expressing either a periplasmic or a membrane-bound nitrate reductase: Does Nap confer a selective advantage during nitrate-limited growth? Biochem. J. **344**, 77-84

[24] Elliott, S. J., Hoke, K. R., Heffron, K., Palak, M., Rothery, R. A., Weiner, J. H. and Armstrong, F. A. (2004) Voltammetric studies of the catalytic mechanism of the respiratory nitrate reductase from *Escherichia coli*: How nitrate reduction and inhibition depend on the oxidation state of the active site. Biochemistry **43**, 799-807

[25] Frangioni, B., Arnoux, P., Sabaty, M., Pignol, D., Bertrand, P., Guigliarelli, B. and Leger, C. (2004) In *Rhodobacter sphaeroides* respiratory nitrate reductase, the kinetics of substrate binding favors intramolecular electron transfer. J. Am. Chem. Soc. **126**, 1328-1329

[26] Dutton, P. L., Wilson, D. F. and Lee, C. P. (1970) Oxidation-reduction potentials of cytochromes in mitochondria. Biochemistry **9**, 5077-5082

[27] Leger, C., Jones, A. K., Albracht, S. P. J. and Armstrong, F. A. (2002) Effect of a dispersion of interfacial electron transfer rates on steady state catalytic

electron transport in NiFe -hydrogenase and other enzymes. J. Phys. Chem. B **106**, 13058-13063

[28] Bell, L. C., Page, M. D., Berks, B. C., Richardson, D. J. and Ferguson, S. J. (1993) Insertion of transposon Tn5 into a structural gene of the membrane-bound nitrate reductase of *Thiosphaera pantotropha* results in anaerobic overexpression of periplasmic nitrate reductase-activity. J. Gen. Microbiol. **139**, 3205-3214

[29] Ellington, M. J. K., Fosdike, W. L. J., Sawers, R. G., Richardson, D. J. and Ferguson, S. J. (2006) Regulation of the nap operon encoding the periplasmic nitrate reductase of *Paracoccus pantotrophus*: Delineation of DNA sequences required for redox control. Arch. Microbiol. **184**, 298-304

[30] Richardson, D. J., Kelly, D. J., Jackson, J. B., Ferguson, S. J. and Alef, K. (1986) Inhibitory effects of myxothiazol and 2-N-heptyl-4-hydroxyquinoline-N-oxide on the auxiliary electron-transport pathways of *Rhodobacter capsulatus*. Arch. Microbiol. **146**, 159-165

[31] Wermuth, B.and Brodbeck, U. (1973) Inhibition of acetylcholinesterase activity by aromatic chelating-agents. Eur. J. Biochem. **35**, 499-506

[32] Cleland, W. (1970) The enzymes: Kinetics and mechanism. New York: Academic Press

[33] Otten, M. F., Reijnders, W. N. M., Bedaux, J. J. M., Westerhoff, H. V., Krab, K. and Van Spanning, R. J. M. (1999) The reduction state of the q-pool regulates the electron flux through the branched respiratory network of *Paracoccus denitrificans*. Eur. J. Biochem. **261**, 767-774

[34] Heffron, K., Leger, C., Rothery, R. A., Weiner, J. H. and Armstrong, F. A. (2001) Determination of an optimal potential window for catalysis by *E. coli* dimethyl sulfoxide reductase and hypothesis on the role of Mo(V) in the reaction pathway. Biochemistry **40**, 3117-3126

[35] Angove, H. C., Cole, J. A., Richardson, D. J. and Butt, J. N. (2002) Protein film voltammetry reveals distinctive fingerprints of nitrite and hydroxylamine reduction by a cytochrome *c* nitrite reductase. J. Biol. Chem. **277**, 23374-23381

[36] Gwyer, J. D., Richardson, D. J. and Butt, J. N. (2005) Diode or tunnel-diode characteristics? Resolving the catalytic consequences of proton coupled

electron transfer in a multi-centered oxidoreductase. J. Am. Chem. Soc. **127**, 14964-14965

[37] Barker, C. D., Reda, T. and Hirst, J. (2007) The flavoprotein subcomplex of complex I (NADH:Ubiquinone oxidoreductase) from bovine heart mitochondria: Insights into the mechanisms of NADH oxidation and NAD^+ reduction from protein film voltammetry. Biochemistry **46**, 3454-3464

[38] Sucheta, A., Ackrell, B. A. C., Cochran, B. and Armstrong, F. A. (1992) Diode-like behavior of a mitochondrial electron-transport enzyme. Nature **356**, 361-362

Table 1 Redox properties of *P. pantotrophus* NapAB

Cofactor	Mid-point Potential (mV)	pH	Spectroscopic Method	Reference
$[4Fe\text{-}4S]^{2+/1+}$	-160	7.4	EPR	[15]
$[4Fe\text{-}4S]^{2+/1+}$	-124 ± 20	6.0	EPR	this work
Hemes	-18 ± 20 77 ± 20	7.0	UV-visible absorption	[9]
Hemes	-30 ± 20	6.0	UV-visible absorption	this work

Figure 1 The respiratory nitrate reductases of *Paracoccus pantotrophus*

Figure 2 PFV of *P. pantotrophus* NapAB

Cyclic voltammograms at pH 6, 8 and 9 as indicated. Consecutive scans recorded in 0, 5, 10, 19, 38, 76, 150 and 300 µM nitrate as indicated by the direction of the solid arrow at the left of each panel. For the pH 6 response in 300 µM nitrate the potentials of E_{cat} and E_{switch} are indicated by open-headed arrows. Buffer-electrolyte: 2 mM neomycin, 100 mM NaCl and 25 mM of either potassium phosphate (pH 6.0), Taps (pH 8.0) or Ches (pH 9.0) at 20 ^{o}C. Scan rate 20 mV s^{-1}, electrode rotation at 3000 rpm.

Figure 3 Characteristic parameters derived from catalytic PFV of NapAB

(**A**) Ratio of the catalytic current at the potential where it reaches its peak value ($i_{cat}^{peak\ E}$) to that at -0.4 V ($i_{cat}^{-0.4V}$) in 2 mM nitrate. (**B**) Maximum catalytic current (i_{max}) magnitude at the peak potential (●) and –0.4 V (□). Lines indicate variation of catalytic current due to ionisation of a single residue with pK_a = 7.8, see text for details. (**C**) Michaelis constants calculated from catalytic currents at the peak potential (●) and -0.4 V (□). (**D**) Values of E_{cat} (●) and E_{switch} (■) for 2 mM nitrate and E_{cat} (○) and E_{switch} (□) for 5 µM nitrate. The line through data for E_{cat} at 2 mM nitrate indicates the variation expected for reduction of a one electron centre with the oxidised state influenced by ionisation of a site with pK_a =7.2. The line through E_{switch} at 2 mM nitrate shows a linear fit to the data with slope -15 mV per pH unit.

Figure 4 Kinetic analysis of catalytic PFV from NapAB

Catalytic currents at the peak potentials (●) and -0.4 V (□) for the voltammograms in Figure 2 presented after correction for signal loss over time. Lines show fits to the Michaelis-Menten equation; $K_M^{peak\ E}$ and $i_{\max}^{peak\ E}$ at pH 6 are 22 µM and 2.67 µA, at pH 8 are 27 µM and 0.98 µA and at pH 9 are 60 µM and 0.51 µA, respectively; $K_M^{-0.4V}$ and $i_{\max}^{-0.4V}$ values at pH 6 are 38 µM and 1.17 µA, at pH 8 are 53 µM and 0.50 µA and at pH 9 are 100 µM and 0.25 µA respectively.

Figure 5 Spectrophotometric analysis of NapAB nitrate reduction

Initial (■) and maximal (●) rates of NapAB dependent nitrate reduction with dithionite reduced methyl viologen as the electron donor. Lines illustrate Michaelis-Menten behaviour with K_M, k_{cat} values of 112 μM, 58 s^{-1} and 176 μM, 104 s^{-1} for the initial and maximal rates respectively. Inset. Absorbance at 600 nm during the spectrophotometric analysis of NapAB activity in 2.7 mM KNO_3 where * indicates enzyme addition to 5.4 nM. Experiments performed in 25 mM Pipes, 100 mM NaCl, pH 7.0 at room temperature.

Figure 6 Nitrate reduction by intact cells of *P. pantotrophus* M6

The solid lines illustrate the nitrate concentration in a stirred suspension of *P. pantotrophus* M6 cells as measured by a nitrate electrode. Pulses of nitrate (70 or 35 μM) were introduced at the times indicated by the arrows. The dashed lines indicate the linear decrease in nitrate concentration from which the maximum rate of nitrate consumption can be derived. Cells were suspended in 10 mM phosphate, 30 mM sodium succinate, 10 mM ammonium sulphate, pH 7 at 30 ˚C.

Figure 7 Inhibition of NapAB nitrate reduction

The solid lines show PFV of NapAB during titration of nitrate into a solution containing (A) 2.5 mM thiocyanate and (B) 2 mM azide. Nitrate concentration increased as 0, 5, 10, 19, 38, 76, 150, 300 and 3000 μM as indicated by the arrows. Broken lines, show the second voltammogram recorded after the nitrate titration and transfer into 2 mM nitrate, no inhibitor. Lineweaver-Burk plots for catalytic currents at -0.40 V (Inset A) thiocyanate concentrations of 0 (○), 2.5 (▲), 5 (●) and 20 (■) mM and (Inset B) azide concentrations of 0.125 (○), 0.5 (▲), 2 (●) and 5 mM (■). Catalytic currents normalised for film coverage in each case. Buffer-electrolyte: 2 mM neomycin, 25 mM potassium phosphate, 100 mM NaCl, pH 6.0, 20 ^{o}C. Scan rate 20 mV s^{-1}, electrode rotation at 3000 rpm.

Figure 8 Schematic representation of the normalised activities of *P. pantotrophus* NapAB (thick line) and NarGH (thin line) together with potentials that may be accessed through modulation of the ubiquinol content (grey) of the cytoplasmic membrane at pH 6 and 7. Data for NarGH activity is taken from [10].

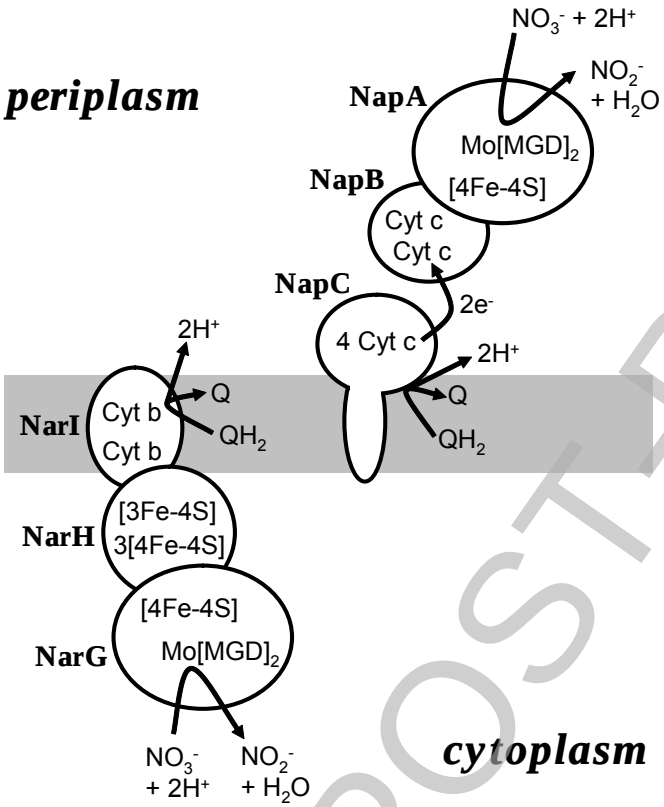

Figure 1

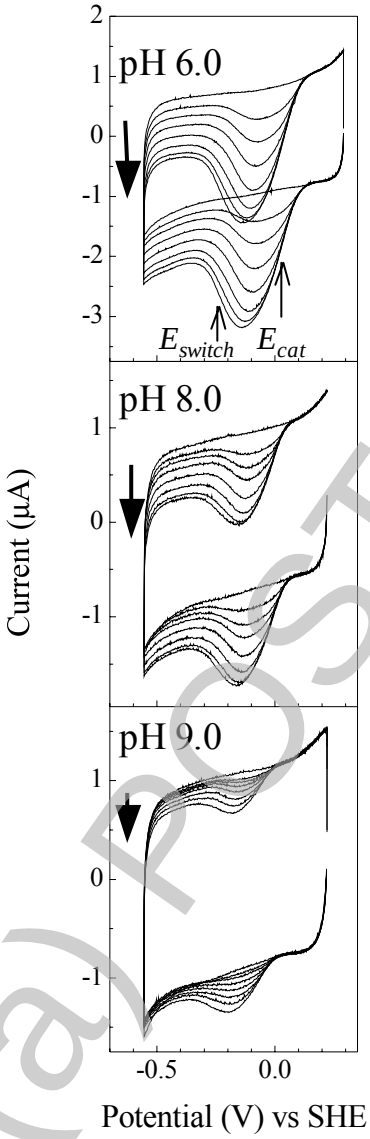

Figure 2

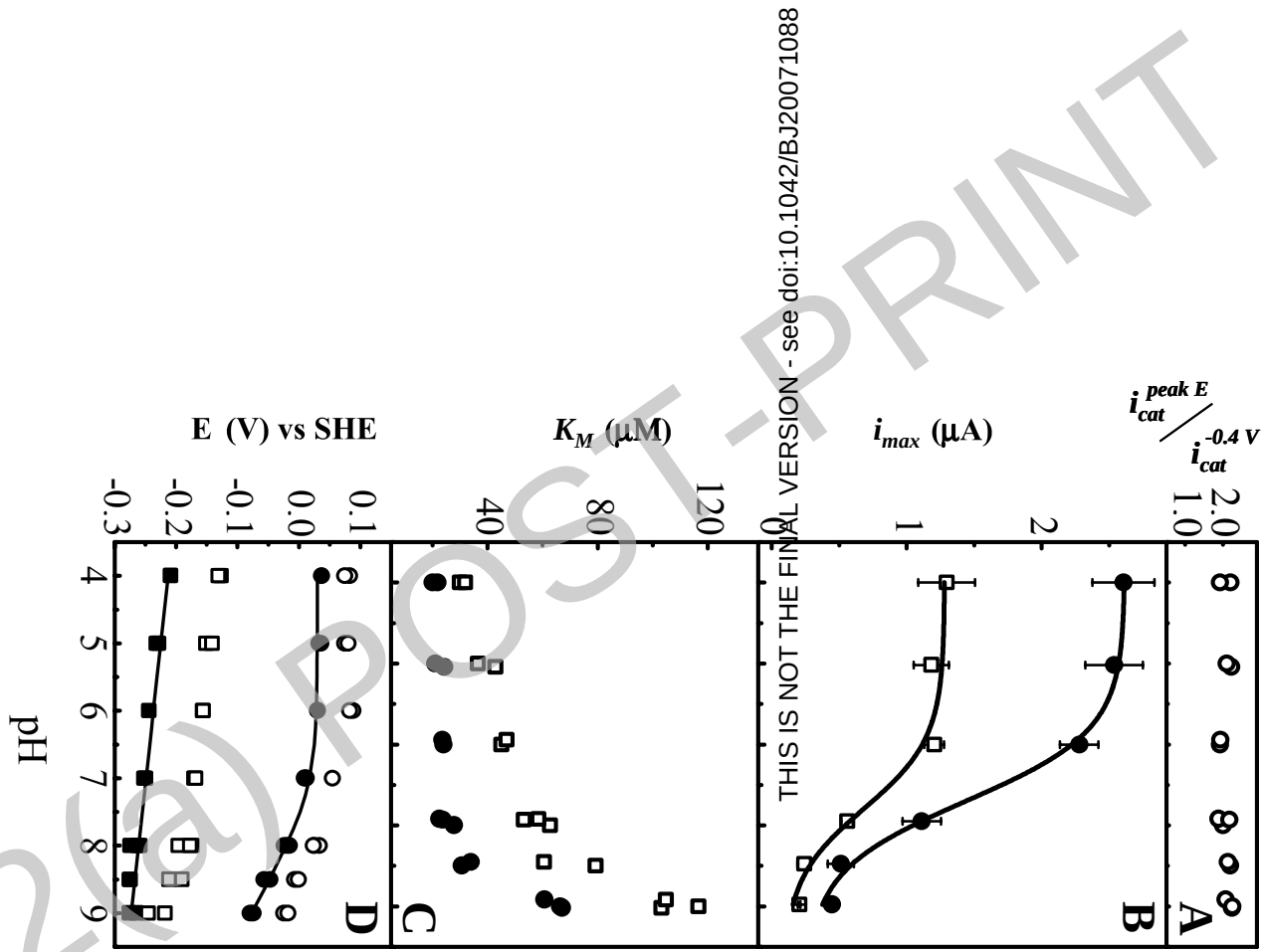

Figure 3

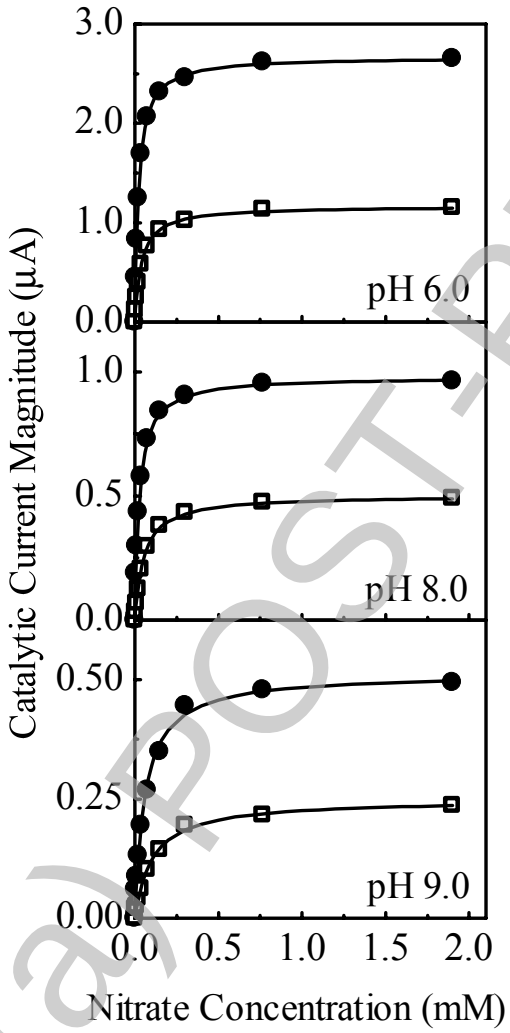

Figure 4

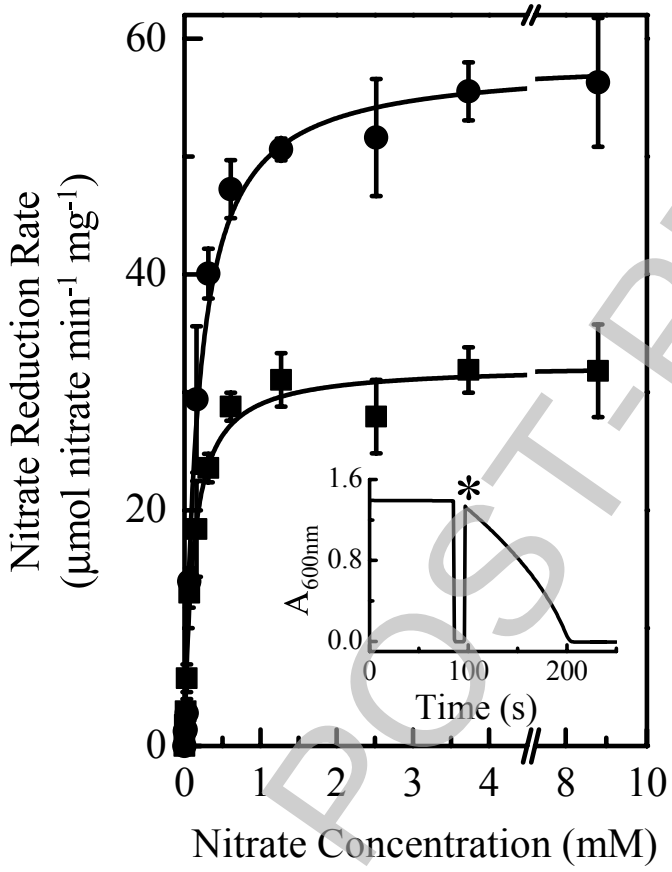

Figure 5

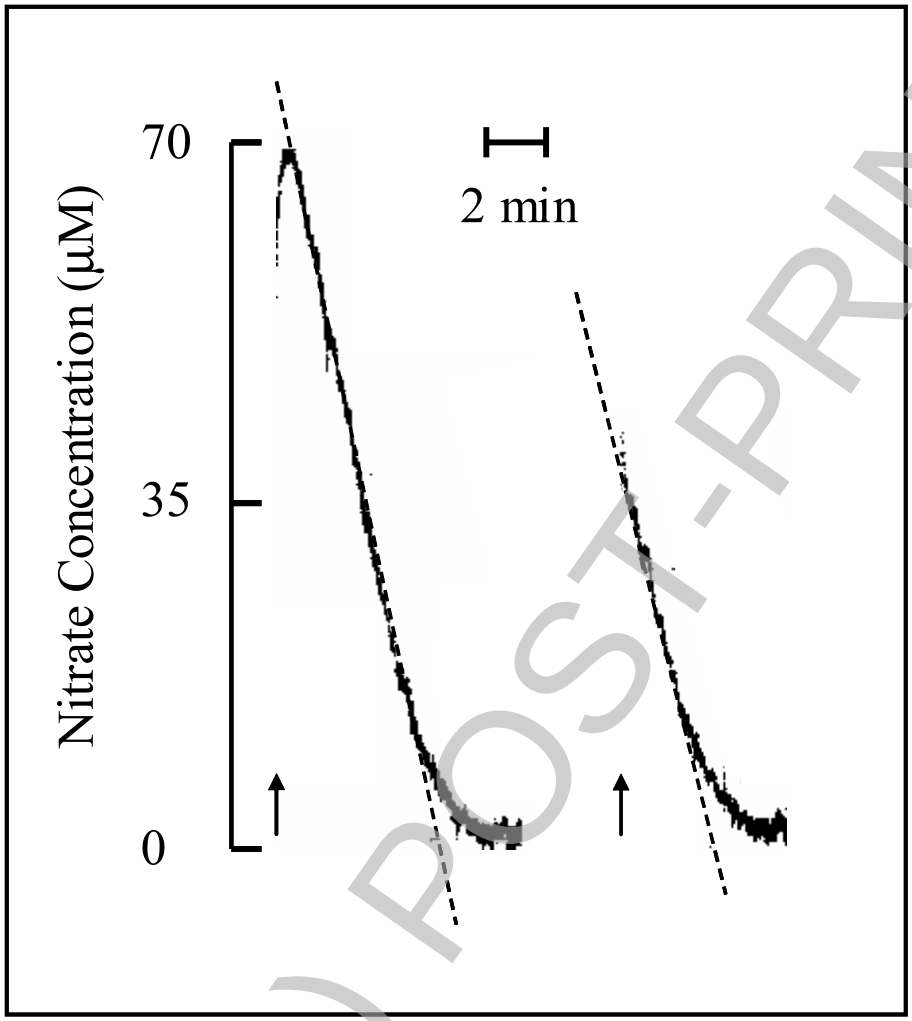

Figure 6

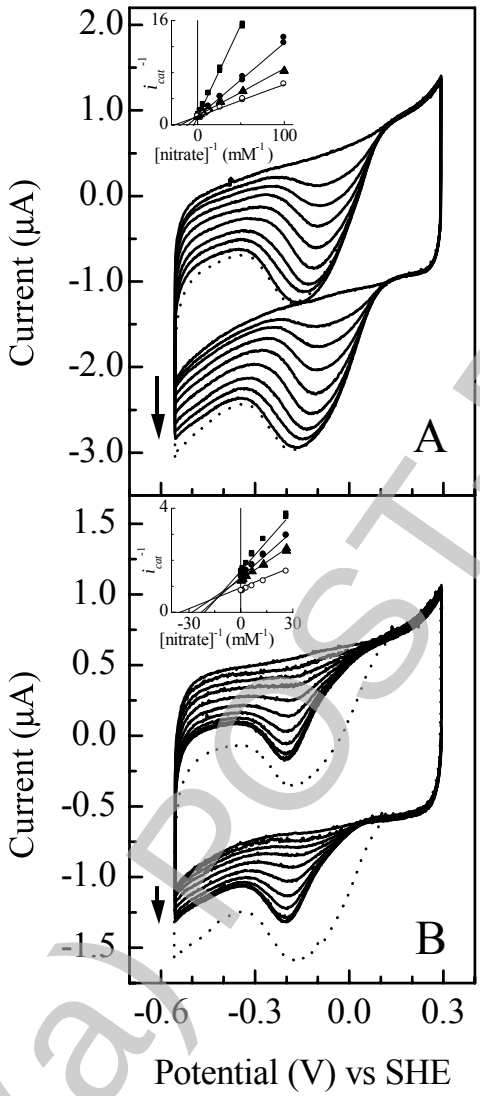

Figure 7

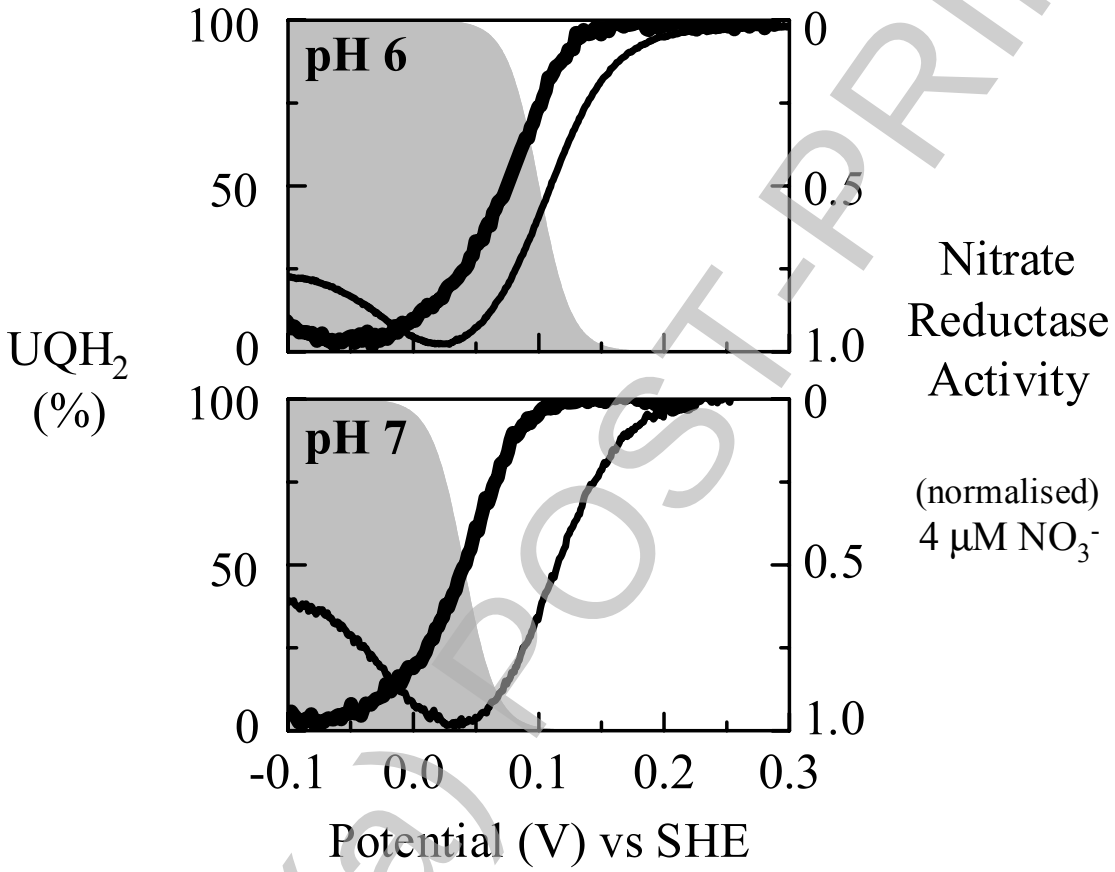

Figure 8